

Low-Temperature Behavior of Biodiesel: Solid–Liquid Phase Diagrams of Binary Mixtures Composed of Fatty Acid Methyl Esters

Mariana C. Costa,[†] Laslo A. D. Boros,[‡] João A. P. Coutinho,[§] M. A. Krähenbühl,[‡] and Antonio J. A. Meirelles^{*,†}

[†]Laboratory EXTRAE, Department of Food Engineering, Faculty of Food Engineering, University of Campinas (UNICAMP), 13083-862 Campinas, São Paulo (SP), Brazil

[‡]Laboratory of Thermodynamic Properties (LPT), Department of Chemical Process, School of Chemical Engineering, University of Campinas (UNICAMP), 13083-970 Campinas, São Paulo (SP), Brazil

[§]Departamento de Química, Centro de Investigação em Materiais Cerâmicos e Compósitos (CICECO), Universidade de Aveiro, 3810-193 Aveiro, Portugal

ABSTRACT: Although biodiesel is being widely used in blends with conventional diesel (Bx) as an automotive fuel, information on its low-temperature behavior is still scarce, in particular concerning the solid–liquid phase behavior of the biodiesel components at temperatures below the cloud point. Although methyl oleate or methyl linoleate are typically components with the highest concentration in the biodiesel, its cloud point is much more influenced by saturated fatty esters because of their higher melting temperatures. The objective of this study is to present a detailed description of the solid–liquid phase diagrams of selected binary mixtures containing the main saturated methyl fatty esters found in biodiesel. The *liquidus* lines and phase behavior below this transition were determined for the following binary mixtures: methyl myristate + methyl palmitate, methyl myristate + methyl stearate, and methyl palmitate + methyl stearate. It will be shown that these systems are not eutectic as previously admitted but, instead, have a complex phase behavior that may have unexpected impacts on the behavior of biodiesel at low temperatures.

1. INTRODUCTION

The increasing population and economic growth of a number of developing countries, conjugated with dwindling petroleum reserves, has amplified the world demand for alternative energies. Moreover, to a large extent, climate changes have been linked to the burning of fossil fuels, which leads to the emission of large quantities of greenhouse gases. In this scenario, it is important to develop new renewable energy sources that can meet the global energy demands without harming the environment.

Biodiesel and bioethanol are among the most promising new alternative fuel sources. Biodiesel is comprised of acyl esters of fatty acids produced by transesterification of oils and fats with short-chain alcohols, commonly methanol or ethanol, in the presence of homogeneous or heterogeneous catalysts, with glycerol as the byproduct.¹ Biodiesel is a biodegradable, nontoxic fuel, with lower pollutant emissions than petroleum fuels and is used in mixtures with conventional petrodiesel around the world.²

The study of the solid–liquid equilibrium (SLE) of biodiesel and/or its components is important to understand biodiesel behavior at low temperatures, because this fuel is more prone to crystallize than conventional diesel as a result of the high content of saturated fatty acid esters. Despite its importance, data on the solid–liquid phase behavior for systems of fatty acid esters are scarce in the literature.^{3–6} Moreover, these studies typically provide only the *liquidus* line and no information on the behavior of the solid phase at temperatures below the cloud point. Only a study by Coutinho et al.⁷ addresses crystallization in biodiesel at temperatures below the cloud point but without considering the phase diagrams of the compounds present. As suggested in our

previous works,^{5,6} the thermograms of binary mixtures of methyl and ethyl fatty esters do not, in general, present the behavior of simple eutectic systems but seem to be as complex as those observed for saturated fatty acids previously studied by our research group.^{8–10} In fact, the present study confirms this complexity by measuring the *liquidus* lines and the phase behavior below this transition for the binary systems composed of methyl myristate + methyl palmitate, methyl myristate + methyl stearate, and methyl palmitate + methyl stearate.

2. MATERIALS AND METHODS

2.1. Materials. Indium (99.999%) certified by TA Instruments, cyclohexane (minimum of 99.99%), and naphthalene (minimum of 99%) from Merck were used for differential scanning calorimetry (DSC) calibration. Methyl tetradecanoate (methyl myristate, CAS number 124-10-7), methyl hexadecanoate (methyl palmitate, CAS number 112-39-0), and methyl octadecanoate (methyl stearate, CAS number 112-61-8), with purity greater than 99% and purchased from Nu-Chek, were used for the experimental measurements with no further purification.

2.2. Methods. Binary mixtures were prepared gravimetrically to contain the entire region of phase diagrams, with varying mole fractions within the range of 0.00–1.00. The samples were melted under a nitrogen atmosphere and constant stirring. Small quantities of each sample (3–6 mg) were thermally treated in DSC (MDSC 2920 TA Instruments) by heating the sample at a rate of 5 K min⁻¹ until 15 K above the melting temperature of the mixture component with the

Received: March 18, 2011

Revised: June 9, 2011

Published: June 13, 2011

Table 1. SLE Data for the Methyl Palmitate + Methyl Stearate System

$x_{\text{palmitate}}$	T_{fus} (K)	T_{eutec} (K)	T_{peritec} (K)	T_{metatec} (K)	$T_{\text{transition}}$ (K)	$T_{\text{transition pure components}}$ (K)
0.0000	314.07					313.59
0.0755	311.18		301.99		295.64	
0.2396	308.14		302.56	304.97	295.56	292.41
0.3415	305.90		302.80		295.12	292.47
0.3889	304.97		302.67		295.57	292.62
0.4864	302.16				295.31	292.58
0.6068	300.79	297.82			295.65	292.85
0.6823	299.86	297.95			294.83	292.36
0.7934	299.42	297.71			294.08	
0.9017	299.76	297.88				
1.0000	303.93					303.04

Table 2. SLE Data for the Methyl Myristate + Methyl Palmitate System

$x_{\text{myristate}}$	T_{fus} (K)	T_{eutec} (K)	T_{peritec} (K)	$T_{\text{metatectic}}$ (K)	$T_{\text{transition}}$ (K)	$T_{\text{transition pure components}}$ (K)
0.0000	303.93					303.12
0.1062	301.74		286.73		296.75	
0.1916	300.26		286.79	288.44	294.54	296.86
0.297	298.32		287.03	288.69	291.95	294.01
0.3976	295.98	285.52	286.95	288.88	290.28	293.84
0.4719	293.99	285.46		288.79		
0.5703	288.09	286.04		289.27		
0.6795	287.14	286.38				
0.7851	286.67	285.67				
0.8638	286.52					
0.8986	289.86	286.8		288.24		
0.9526	291.22			288.44	289.81	
1.0000	292.98					292.48

higher melting temperature. The sample was maintained at this temperature for 20 min and was then cooled at a rate of 1 K min⁻¹ to a temperature of 25 K below the melting temperature of the mixture component with the lower melting temperature. After 30 min at this lower temperature, the heating was again started for data collection at a heating rate of 1 K min⁻¹ until complete melting of the sample.

A Leica optical microscope, model DM LM, equipped with a heating stage, model FP82HT (Mettler Toledo), was also used for helping in the characterization of the transitions observed below the *liquidus* line. To be analyzed in the optical microscope, the samples were placed on a glass coverslip, which in turn was placed, one by one, into the heating stage. The heating stage with the sample was put in the optical microscope in the light pathway. Samples were heated at a rate of 0.1 K min⁻¹. The temperature control was performed with the DSC Mettler Toledo FP 90.

3. RESULTS AND DISCUSSION

The melting temperatures and transition temperatures observed under the *liquidus* line for each studied system are presented in Tables 1–3. Thermograms obtained for the methyl palmitate + methyl stearate system are shown in Figure 1. The first thermogram was obtained for pure methyl stearate, $x_{\text{palmitate}} = 0.00$. In this thermogram, with the inset of the enlarged curve presented in Figure 1b, it is possible to note the existence of two peaks, as indicated by the arrows. The first peak, at lower temperature, is attributed to a phase transition of the pure component, probably a polymorphic transition, and the

Table 3. SLE Data for the Methyl Myristate + Methyl Stearate System

$x_{\text{myristate}}$	T_{fus} (K)	T_{eutec} (K)	$T_{\text{transition pure components}}$ (K)
0.0000	314.07		313.59
0.1235	310.74	287.12	
0.1975	309.39	287.32	
0.3053	307.67	287.24	
0.4239	305.5	287.34	
0.5547	302.22	287.39	
0.5711	301.40	287.30	
0.6694	298.63	287.64	
0.7613	293.95	287.86	
0.8594	288.67	287.35	
0.9109	289.19	287.18	
0.9445	290.46	288.19	
1.0000	292.98		292.48

second one, at a slightly higher temperature, is attributed to complete melting of methyl stearate.

With the increase of the methyl palmitate content in the mixture, the thermograms became more complex with a series of overlapped peaks. It is possible to observe five overlapped peaks for $x_{\text{palmitate}} \approx 0.20$. The peak at the highest temperature, 308 K, is resultant of the melting of the sample. The peak located at the

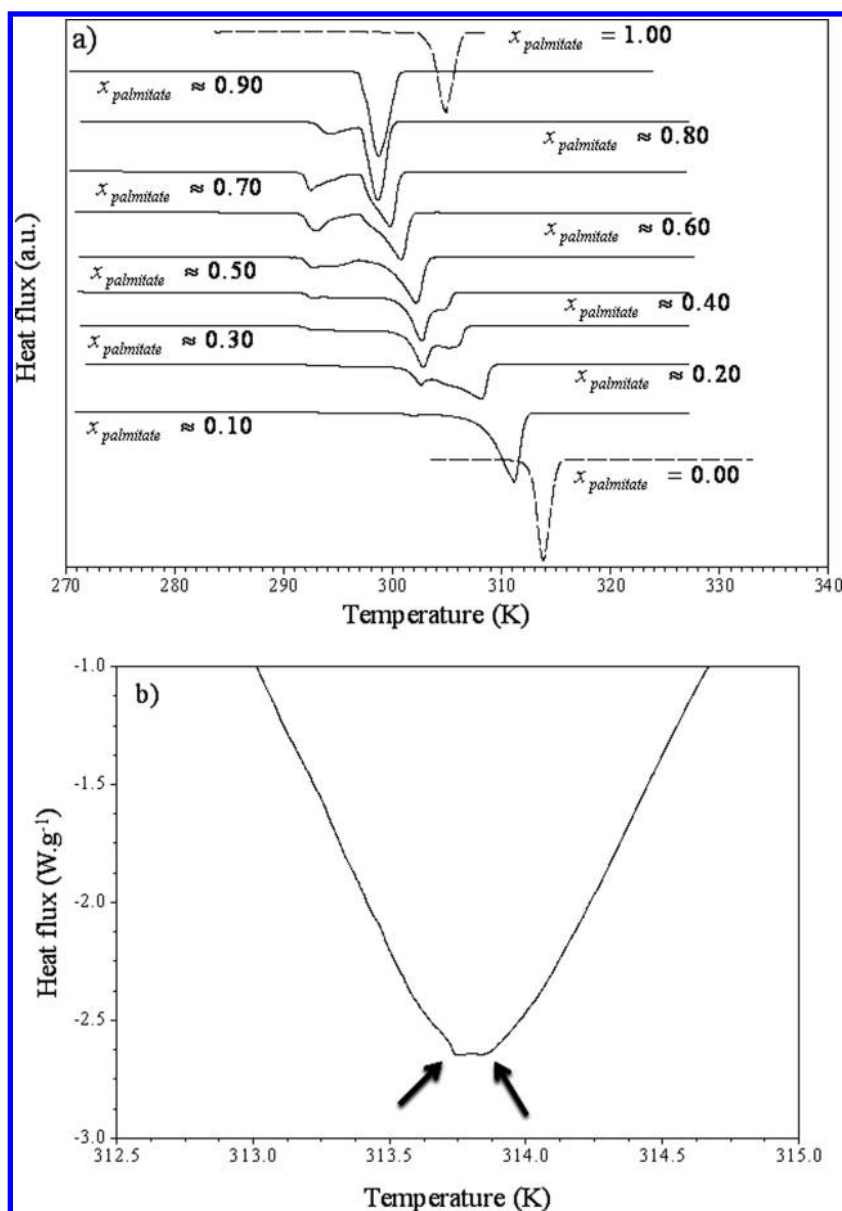


Figure 1. (a) Thermograms of the methyl palmitate + methyl stearate system. (b) Inset of the thermogram for pure methyl stearate ($x_{\text{palmitate}} = 0.00$).

intermediate temperature, roughly 302.5 K, is attributed to a peritectic reaction, and the peak observed at approximately 305 K can be attributed to the metatectic reaction taking place a few degrees above the peritectic temperature, similar to what was observed for the systems formed by saturated fatty acids.^{8–10} The other two peaks observed for this composition, at around 295.5 and 292.4 K, are attributed to solid–solid polymorphic transitions that are often observed in systems with long alkyl chains, particularly in fatty acids and esters. Conclusive information on such transitions would require other analytical techniques, such as X-ray diffraction, that are outside the scope of this work.

As shown in Figure 1a, the increase in the methyl palmitate concentration causes a decrease of the melting temperature, represented by the higher temperature peak for all compositions up to $x_{\text{palmitate}} \approx 0.90$, which is approximately the eutectic composition. For compositions greater than $x_{\text{palmitate}} \approx 0.90$, the melting temperature increases again. With the increase in the

methyl palmitate concentration, the melting peak intensity decreases and tends to overlap with the peak attributed to the peritectic reaction. This peak of the peritectic reaction, in turn, becomes more intense until reaching the composition of $x_{\text{palmitate}} \approx 0.50$, where the reactions overlap and a single peak is observed. At greater composition, the peak of the peritectic reaction is no longer observed. For compositions greater than $x_{\text{palmitate}} = 0.50$, a small peak at a temperature around 298 K can be observed in the thermograms. This peak is attributed to the eutectic reaction and becomes more defined and intense with an increase of the methyl palmitate concentration in the sample. Finally, for pure methyl palmitate, two overlapped peaks, as for pure methyl stearate, are observed. The phase diagram of the methyl palmitate + methyl stearate system, with all phase transitions observed by DSC, is shown in Figure 2. It may be tempting to adopt a simple interpretation of the phase diagram as eutectic with one peritectic point, as suggested in Figure 2, but the reality is far more complex and exciting.

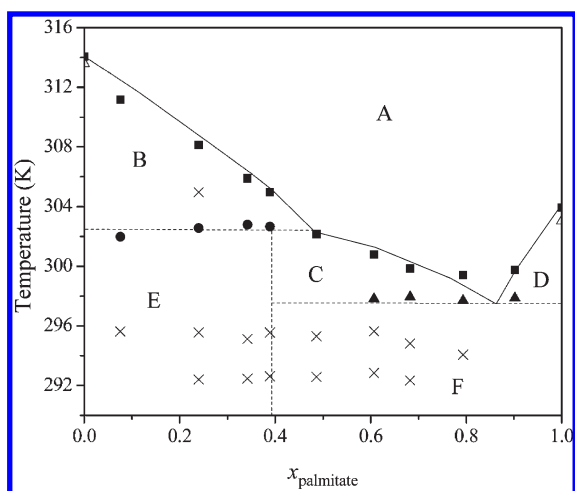


Figure 2. Phase diagram of the methyl palmitate + methyl stearate system: (■) melting temperature, (●) peritectic temperature, (▲) eutectic temperature, (×) solid–solid or solid–liquid transition temperatures, and (△) transition temperature of the pure components.

This simplified version of the phase diagram can be shown to be incorrect if the heating of one sample is performed under an optical microscope with polarized light, as presented in Figure 3 for a mixture at $x_{\text{palmitate}} \approx 0.20$, using a heating rate of 0.1 K min^{-1} . Here, it can be observed that the image of the sample obtained at 298.15 K indicates that it is completely solid, shown by the irregular shape of the crystals. When temperature is increased to 303.15 and 304.15 K, the fringes of the crystals, especially those indicated by arrows, become rounded, with this effect being more pronounced at the temperature of 304.15 K. The rounder shape of the crystals indicates the presence of liquid in the coverslip, and up to this temperature, the amount of liquid observed increases with the temperature as expected. However, above this point, a small temperature increase to 304.65 K shows recrystallization of a part of the liquid phase, indicated by the large arrow. Recrystallization is noted because of the contraction of the fluid as it crystallizes, and the material also becomes slightly darker when compared to what was observed in the previous images. A further increase of the temperature by 1 to 305.65 K shows no significant change in the crystals, only an expansion indicating that the region of recrystallization is very small. The image obtained at 307.15 K shows a significant amount of liquid with small crystals, and the complete melting takes place at approximately 1 K above this temperature. The recrystallization phenomenon observed here at 304.65 K and previously observed for fatty acid systems^{8–10} can be explained by the presence of a metatectic reaction $\gamma \leftrightarrow \alpha + l$, an isothermal reversible reaction of a solid mixture (γ), which turns into a different solid phase (α) plus a liquid phase (l) during cooling of a system.¹¹

Tamman's plot, shown in Figure 4, represents the enthalpy variation of each isothermal peritectic and eutectic reaction, with the sample composition. Chernik¹² showed that this plot can be used to delimit the biphasic regions of a phase diagram. As expected, the enthalpy values of the peritectic and eutectic reactions increased linearly until the exact composition of the eutectic and peritectic points. For compositions greater than the eutectic or peritectic points, the enthalpies also decrease linearly until crossing the composition axis at its extremities for a phase diagram with no solid solution formation or at the concentration where the solid solution appears.

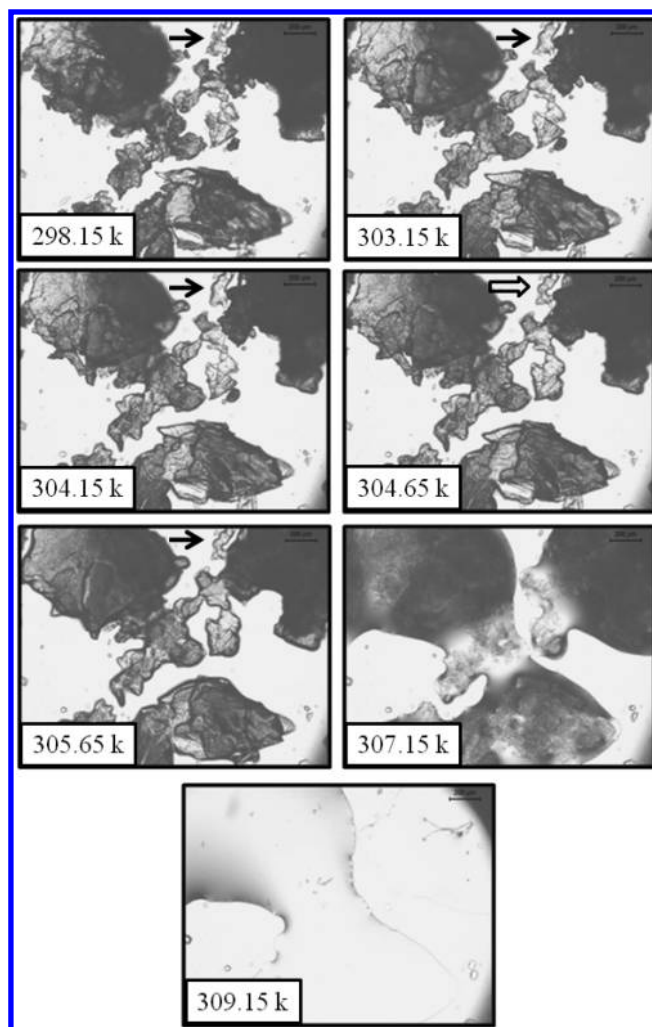


Figure 3. Optical images of the methyl palmitate + methyl stearate system obtained at $x_{\text{palmitate}} \approx 0.20$.

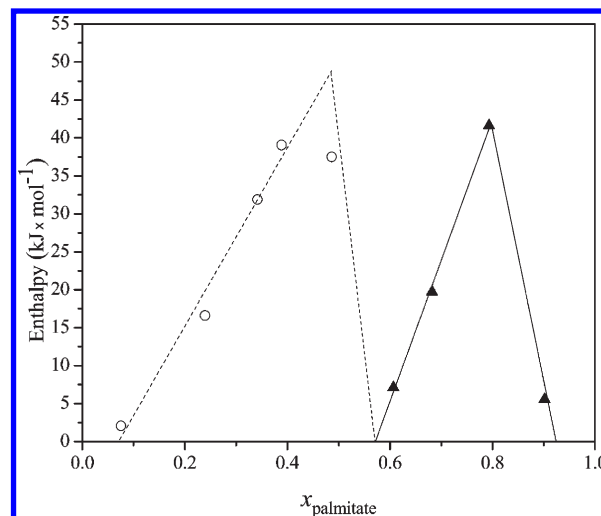


Figure 4. Tamman's plot of the methyl palmitate + methyl stearate system: (▲) enthalpy of the eutectic reaction and (○) enthalpy of the peritectic reaction. Dotted and solid lines are linear fits to the enthalpy values.

The results reported in Figure 4 suggest that solid solutions must be formed at the extremities of the phase diagram below compositions of $x_{\text{palmitate}} \approx 0.04$ and above $x_{\text{palmitate}} \approx 0.96$, respectively. The microscope observations presented in Figure 3 and the results of the Tamman plot show that the simplistic interpretation of the phase diagram for this system shown in Figure 2 is not correct. It thus requires a more comprehensive description of the phase diagram that takes into account all information gathered. Supported by the results of previous studies for SLE phase diagrams of saturated fatty acids,^{8–10} the best interpretation for the DSC thermograms, Tamman plot, and

microscope observations is a phase diagram divided into 14 regions of equilibria, with two metatectic invariant points, presented in Figure 5. It shows the following: (i) four regions of SSE, $C^{e,p} + C$, $C^{e,p} + C_h^e$, $C + C^{p,e}$, and $C^{p,e} + C_h^p$; (ii) five regions of SLE, $C^{e,p} + l$, $C_h^e + l$, $C + l$, $C^{p,e} + l$, and $C_h^p + l$; and (iii) five monophasic regions under the *liquidus* line, $C^{e,p}$, C_h^e , $C^{p,e}$, C_h^p , and C .

Thermograms of the methyl myristate + methyl palmitate system are presented in Figure 6. It can be observed that the thermograms up to $x_{\text{myristate}} \approx 0.47$ exhibit overlapped peaks in the temperature range between 285 and 295 K and a well-defined

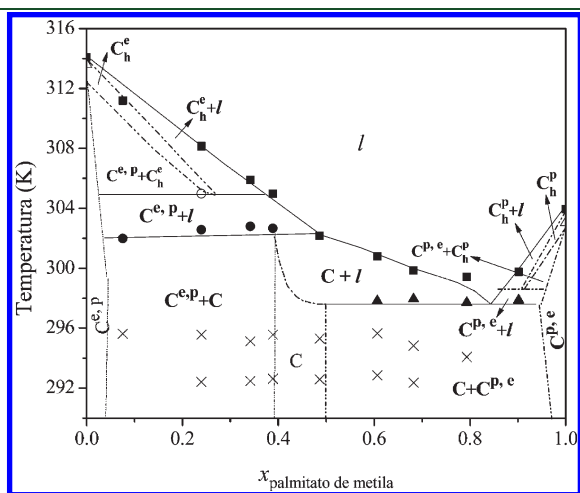


Figure 5. Complete phase diagram of the methyl palmitate + methyl stearate system: (■) melting temperature, (▲) eutectic temperature, (●) peritectic temperature, (○) metatectic temperature, (×) solid–solid transition temperatures, and (△) transition temperature of the pure components.

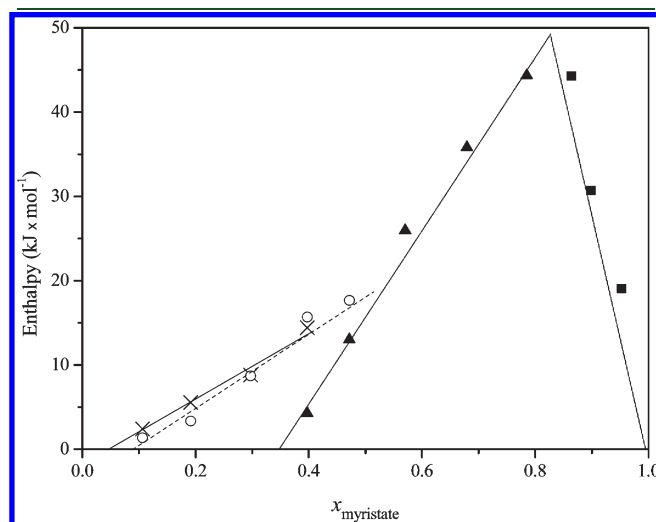


Figure 7. Tamman plot of the methyl myristate + methyl palmitate system: (▲) enthalpy of the eutectic reaction, (○) enthalpy of the peritectic reaction, and (×) enthalpy of the metatectic reaction. Dotted and solid lines are linear fits to the enthalpy values.

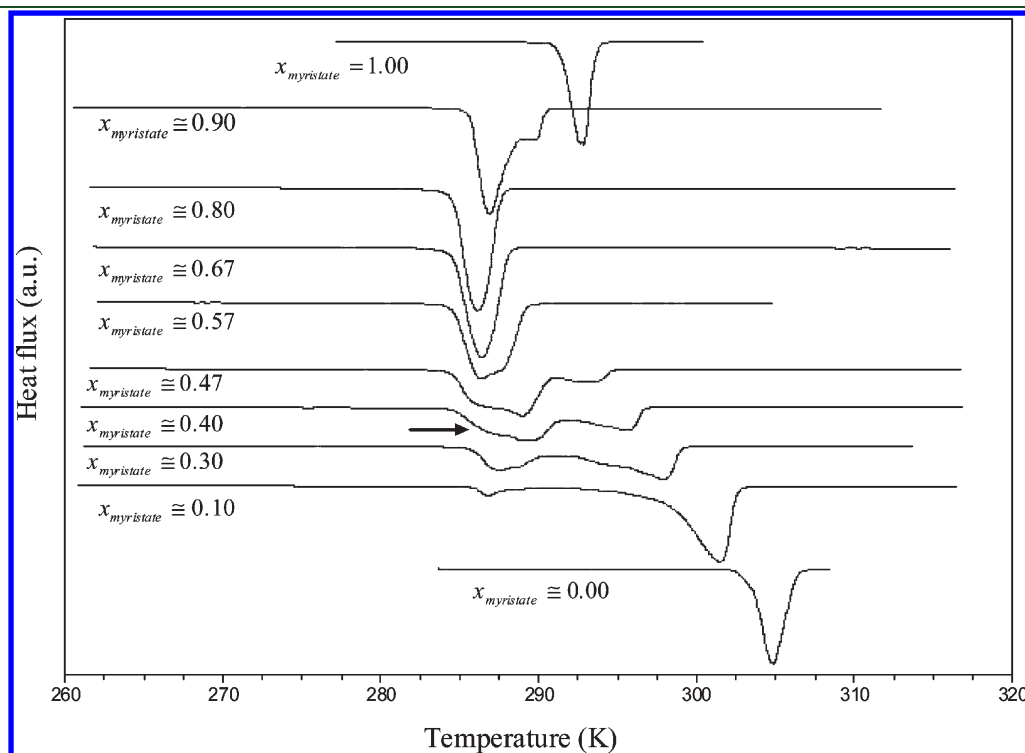


Figure 6. Thermograms of the methyl myristate + methyl palmitate system.

peak at higher temperatures attributed to the melting of the sample. In the thermogram for $x_{\text{myristate}} \cong 0.40$, a very small peak, indicated in Figure 6 by an arrow, appears at low temperatures. For compositions higher than $x_{\text{myristate}} \cong 0.40$, this peak becomes more intense and individualized. This peak seems to be related to the eutectic reaction, suggesting that this transition takes place at 285.5 K and only for methyl myristate concentrations above 0.40.

The Tamman plot for the eutectic reaction and the other transition observed for compositions lower than $x_{\text{myristate}} \cong 0.47$ is shown in Figure 7. It confirms that the eutectic reaction takes place only for compositions above $x_{\text{myristate}} \cong 0.40$ and also shows that the overlapped transitions observed for compositions below $x_{\text{myristate}} \cong 0.47$ are also important events, which are interpreted here as the peritectic and metatectic reactions in order of increased temperature. Unfortunately, these two transitions take place in a very narrow temperature range, making their confirmation very difficult using microscopy. Nevertheless, the

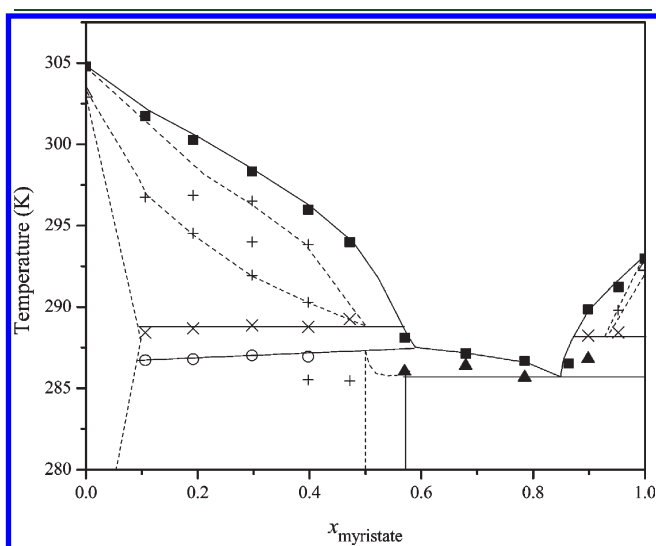


Figure 8. Phase diagram of the methyl myristate + methyl palmitate system: (■) melting temperature, (▲) eutectic temperature, (○) peritectic temperature, (×) metatectic temperature, (+) solid–solid or solid–liquid transition temperatures, and (△) transition temperature of the pure components.

interpretation of the phase diagram of the methyl myristate + methyl palmitate system is presented in Figure 8, displaying a similarity to that of the methyl palmitate + methyl stearate system, as expected. In the thermograms, it was possible to observe other phase transitions within the range between the *liquidus* line and the metatectic reaction, but they could not be fully identified in this work. They may be related to solid–solid transitions of polymorphs.

The last system studied in this work, methyl myristate + methyl stearate, exhibits a different behavior from the previous two because of the large difference in alkyl chain lengths between the two esters. In this system, only an eutectic point can be observed, as shown in panels a and b of Figure 9. Figure 9a presents the phase diagram of the methyl myristate + methyl stearate system, and Figure 9b presents the Tamman plot for the same system. When the three phase diagrams studied here are compared, it is possible to note their differences. The phase diagrams of the methyl palmitate + methyl stearate and methyl myristate + methyl palmitate systems present multiple phase transitions below the *liquidus* line, as described above, related to the presence of peritectic and metatectic reactions, while in this system, no such transitions are observed. The absence of transitions makes interpretation of the thermograms much easier and is an indication of the occurrence of a simple eutectic system that is confirmed by the Tamman plot presented in Figure 9b. In fact, this Tamman plot exhibits the behavior mentioned in the literature for a simple eutectic system.¹²

In our previous study concerning the solid–liquid phase diagrams of binary saturated fatty acid mixtures,^{8–10} the occurrence of eutectic, peritectic, and metatectic reactions was observed in the systems with a difference of two and four carbon atoms between the carbon chains of the mixture. The presence of these reactions was also observed for some systems with a difference of six carbon atoms. In this study, we show that the same complexity in the phase diagrams is observed for binary mixtures of fatty acid methyl esters (FAMEs), but in this case, the difference between the carbon chains plays a more important role. For FAMEs, the behavior observed for binary systems differing by four carbon atoms, methyl myristate + methyl stearate, was simpler than that observed for binary mixtures of fatty acids with differences of six carbons. The FAME phase diagrams for systems differing by two carbon atoms present a

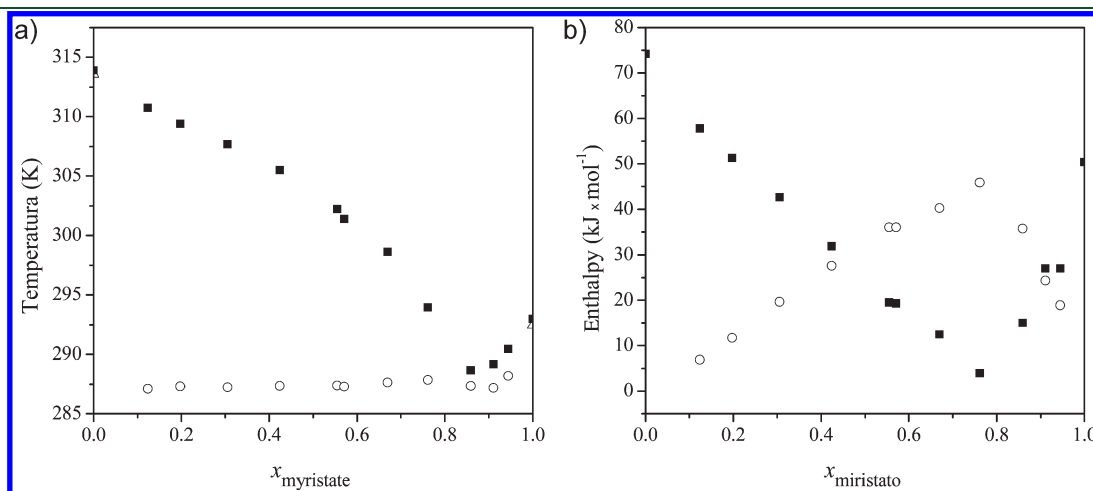


Figure 9. (a) Phase diagram of the methyl myristate + methyl stearate system. (b) Tamman plot of the same system: (■) melting temperature, (○) eutectic temperature, and (△) transition temperature of the pure components.

structure similar to what was observed for fatty acid systems differing by two or four carbons when the components of the mixtures have long alkyl chains, such as in the methyl palmitate + methyl stearate system. In contrast, when the mixture components have shorter chain lengths, such as in the methyl myristate + methyl palmitate system, the phase behavior is similar to that observed for fatty acid systems with a difference of six carbon atoms between the carbon chains. All systems seem to indicate that differences in the alkyl chain size play a more important role on the methyl esters than on the fatty acids.

The results reported here have important implications on the low temperature of biodiesels. Being that methyl palmitate and methyl stearate are the esters responsible for crystal formation at low temperatures that leads to the cloud point, pour point, and cold filter plugging point (CFPP), its binary phase diagram is directly implicated in defining the values of these properties. The presence of the metatectic reaction is responsible for the formation of a more significant quantity of solids below the cloud point than would be anticipated if a simple eutectic or peritectic system were present. The knowledge of these phase diagrams and the detailed behavior of these mixtures below the cloud point should aid in optimizing the blends for efficient operation at low temperatures and the design of additives to prevent crystallization or gelling of the biofuel.

4. CONCLUSION

The solid–liquid phase diagrams of methyl myristate + methyl palmitate, methyl palmitate + methyl stearate, and methyl myristate + methyl stearate were determined by DSC. The optical microscopy was employed to verify the solid liquid boundaries of the methyl palmitate + methyl stearate system. Eutectic, peritectic, and also metatectic reactions were observed in the methyl myristate + methyl palmitate and methyl palmitate + methyl stearate systems. The presence of such reactions in the phase diagrams implies a more significant solid portion in the region comprised between the *liquidus* line and the peritectic temperature. Just the eutectic reaction was observed in the system formed by methyl myristate + methyl stearate.

■ AUTHOR INFORMATION

Corresponding Author

*Telephone: +55-19-3521-4037. Fax: +55-19-3521-4027. E-mail: tomze@fea.unicamp.br.

■ ACKNOWLEDGMENT

The authors are grateful to CNPq (304495/2010-7 and 480992/2009-6), FAPESP (08/09502-0 and 08/56258-8), CAPES, and FAEPEX/UNICAMP for their financial support.

■ REFERENCES

- (1) Demirbas, A. Biodiesel production from vegetable oils via catalytic and non-catalytic supercritical methanol transesterification methods. *Prog. Energy Combust. Sci.* **2005**, *31* (5–6), 466–487.
- (2) Knothe, G.; Gerpen, J. V.; Krahl, J.; Ramos, L. P. *Manual de Biodiesel*; Edgard Blücher: São Paulo, Brazil, 2006.
- (3) Lopes, J. C. A.; Boros, L.; Krahenbuhl, M. A.; Meirelles, A. J. A.; Daridon, J. L.; Pauly, J.; Marrucho, I. M.; Coutinho, J. A. P. Prediction of cloud points of biodiesel. *Energy Fuels* **2008**, *22* (2), 747–752.

- (4) Imahara, H.; Minami, E.; Saka, S. Thermodynamic study on cloud point of biodiesel with its fatty acid composition. *Fuel* **2006**, *85* (12–13), 1666–1670.

- (5) Boros, L.; Batista, M. L. S.; Vaz, R. V.; Figueiredo, B. R.; Fernandes, V. F. S.; Costa, M. C.; Krahenbuhl, M. A.; Meirelles, A. J. A.; Coutinho, J. A. P. Crystallization behavior of mixtures of fatty acid ethyl esters with ethyl stearate. *Energy Fuels* **2009**, *23*, 4625–4629.

- (6) Costa, M. C.; Boros, L.; Batista, M. L. S.; Coutinho, J. A. P.; Krähenbühl, M. A.; Meirelles, A. J. A. Phase diagrams of mixtures of ethyl palmitate with fatty acid ethyl esters. *Fuel Process. Technol.* **2011**.

- (7) Coutinho, J. A. P.; Goncalves, M.; Pratas, M. J.; Batista, M. L. S.; Fernandes, V. F. S.; Pauly, J.; Daridon, J. L. Measurement and modeling of biodiesel cold-flow properties. *Energy Fuels* **2010**, *24*, 2667–2674.

- (8) Costa, M. C.; Rolemberg, M. P.; Meirelles, A. J. A.; Coutinho, J. A. P.; Krahenbuhl, M. A. The solid–liquid phase diagrams of binary mixtures of even saturated fatty acids differing by six carbon atoms. *Thermochim. Acta* **2009**, *496* (1–2), 30–37.

- (9) Costa, M. C.; Sardo, M.; Rolemberg, M. P.; Coutinho, J. A. P.; Meirelles, A. J. A.; Ribeiro-Claro, P.; Krähenbühl, M. A. The solid–liquid phase diagrams of binary mixtures of consecutive, even saturated fatty acids. *Chem. Phys. Lipids* **2009**, *160*, 85–97.

- (10) Costa, M. C.; Sardo, M.; Rolemberg, M. P.; Coutinho, J. A. P.; Meirelles, A. J. A.; Ribeiro-Claro, P.; Krähenbühl, M. A. The solid–liquid phase diagrams of binary mixtures of consecutive, even saturated fatty acids: Differing by four carbon atoms. *Chem. Phys. Lipids* **2009**, *157*, 40–50.

- (11) Gamsjager, H.; Lorimer, J. W.; Scharlin, P.; Shaw, D. G. Glossary of terms related to solubility. *Pure Appl. Chem.* **2008**, *80* (2), 233–276.

- (12) Chernik, G. G. Phase equilibria in phospholipid water systems. *Adv. Colloid Interface Sci.* **1995**, *61*, 65–129.

■ NOTE ADDED AFTER ASAP PUBLICATION

Tables 2 and 3 have been revised from their original version published on the Web on June 13, 2011. The revised version was published on the Web on July 5, 2011.